Spin precession in lateral all-metal spin valves: Experimental observation and theoretical description

Alexander van Staa, Jeannette Wulfhorst,* Andreas Vogel, Ulrich Merkt, and Guido Meier
Institut für Angewandte Physik und Zentrum für Mikrostrukturforschung, Universität Hamburg, Jungiusstrasse 11, 20355 Hamburg
(Received 23 August 2007; published 10 June 2008)

Mesoscopic all-metal spin-valve devices containing two ferromagnetic permalloy electrodes and an interconnecting aluminum strip have been studied experimentally and theoretically in nonlocal geometry. Spin-valve devices have been fabricated by thermal evaporation of permalloy electrodes, formation of tunnel barriers by natural oxidation in air or in pure oxygen, and subsequent deposition of an aluminum strip on top of the electrodes. Transport measurements at temperatures of liquid helium have been performed. Spin-dependent phenomena, namely the nonlocal spin-valve effect and spin precession, are observed. A theoretical description of spin-dependent transport is presented including spin diffusion, spin relaxation, spin precession, and tunnel barriers at the interfaces between the electrodes and the aluminum strip. From the comparison of the experimentally observed spin precession to the theoretical description, we obtain a spin-relaxation time of 111 ps and a spin-relaxation length of 1034 nm in aluminum.

DOI: 10.1103/PhysRevB.77.214416 PACS number(s): 72.25.Ba, 72.25.Mk, 72.25.Rb, 73.23.−b

I. INTRODUCTION

In spintronics all-electrical injection and detection of spin-polarized currents in normal metals or semiconductors are the main challenges. After injection the spin-diffusion length defines the scale of coherence. Johnson and Silsbee[1,2] have been the first who showed spin injection and detection in aluminum in 1985 and gave a theoretical description of the phenomena.[3] Since their pioneering work there has been a growing interest in ferromagnet/normal metal hybrid devices.[4–21] Spin-polarized currents have been used in mesoscopic spin-valve devices to demonstrate the spin-valve effect,[4,5,7,9,11,12,15,17,18,20] spin accumulation,[8,14] spin precession,[6,13] and magnetization reversal of small ferromagnetic particles.[16] Many of these experiments have utilized nonlocal measurement geometries. The interface quality between the ferromagnetic electrodes and the normal metal is crucial for a successful spin injection and a high magnitude of the output signal. Especially for magnetization switching processes, which are of rapidly growing interest for future storage devices, highly polarized currents are necessary. Tunnel barriers, which avoid spin scattering, are well known to increase the spin-injection rate[22] and thus to provide the high currents required for such devices. In this paper we present electrical transport experiments on lateral spin valves in nonlocal geometry, observe the spin-valve effect and spin precession, and give a theoretical description of spin transport in the diffusive regime. The model describes our mesoscopic spin-valve devices for the nonlocal geometry including spin diffusion, spin relaxation, spin precession, and tunnel barriers at the interfaces.

The paper is organized as follows. In Sec. II we introduce the diffusion equations in one dimension regarding spin relaxation and spin precession. With this model these spin-dependent phenomena in a spin-valve device consisting of two ferromagnetic electrodes, an interconnecting normal-metal strip and tunnel barriers at the interfaces between ferromagnets and the normal metal are calculated and discussed. The experimental realization of spin-valve devices is described in Sec. III. Measurements of the nonlocal spin-valve effect, minor loops, and spin precession are presented and compared to the theoretical description in Sec. IV. Results are discussed in Sec. V. We conclude with a summary in Sec. VI.

II. THEORY

The theoretical description of spin-dependent effects is based on diffusive transport in one dimension. Assuming that the spin-diffusion length λ is large in comparison to the mean free path of the electrons, the transport of spin-up and spin-down electrons can be described independently.[23] According to the idea of Johnson and Silsbee,[3] we integrate spin precession, spin relaxation, spin diffusion, and tunnel barriers in the diffusion equations and solve them for the geometry of the present experiment. The chemical potentials μ of the electrons in the case of no charge current are derived following the approach of Kimura *et al.*[9] The current in a ferromagnet exhibits the bulk spin polarization α, which yields a spin current $I_S=\alpha I_C$ when I_C is the charge current. At the boundaries of the ferromagnetic materials, i.e., at the interfaces to the normal metal, a source of spin current is assumed. The spin current diffuses according to their conductivities partly into the ferromagnet and the normal metal. As a result the spin current at the interface within the ferromagnet is reduced in comparison to the bulk material, and within the normal metal a spin current is produced. A concomitant splitting of the electrochemical potential for spin-up and spin-down electrons occurs.[23,24] The charge current has no influence on the spin-dependent effects treated in the present work and is therefore not regarded.

First the derivation of the diffusion equations for the chemical potentials is described regarding spin-relaxation processes, spin precession, and spin diffusion in a normal metal (N). The difference of the excess particle densities of the spin-up and spin-down electrons is defined as $\Delta n=n_\uparrow-n_\downarrow$, which we address as spin splitting in the following. In our description no space direction is preferred, i.e., spin-up

and spin-down electrons can point in all three dimensions, which leads to the spin splittings Δn_x, Δn_y, and Δn_z. The indices x, y, and z indicate the space direction. Spin precession occurs in an external magnetic field $\vec{H}$, which points into the z direction. Thus the time evolution of the spin splittings can be written as $\partial \Delta n_x/\partial t = \omega_L \Delta n_y$, $\partial \Delta n_y/\partial t = -\omega_L \Delta n_x$, and $\partial \Delta n_z/\partial t = 0$ with the Larmor frequency $\omega_L = g\mu_B \mu_0 H/\hbar$, the gyromagnetic factor g of the free electron, and the Bohr magneton μ_B. Spin relaxation is described by $\partial \Delta n/\partial t = -\Delta n/\tau_N$, where τ_N is the spin-relaxation time. Spin diffusion is given by $\partial \Delta n/\partial t = D_N \partial^2 \Delta n/\partial x^2$, where D_N is the diffusion constant. Thus, in the steady state the diffusion equations read

$$\frac{\partial \Delta n_x}{\partial t} = \omega_L \Delta n_y - \frac{\Delta n_x}{\tau_N} + D_N \frac{\partial^2 \Delta n_x}{\partial x^2} = 0, \tag{1}$$

$$\frac{\partial \Delta n_y}{\partial t} = -\omega_L \Delta n_x - \frac{\Delta n_y}{\tau_N} + D_N \frac{\partial^2 \Delta n_y}{\partial x^2} = 0, \tag{2}$$

$$\frac{\partial \Delta n_z}{\partial t} = -\frac{\Delta n_z}{\tau_N} + D_N \frac{\partial^2 \Delta n_z}{\partial x^2} = 0. \tag{3}$$

The difference of the chemical potentials of the spin-up and the spin-down electrons is proportional to the spin splitting Δn and to the concomitant voltage difference ΔV_N,

$$\frac{\mu_{N\uparrow} - \mu_{N\downarrow}}{e} = \frac{2eD_N}{\sigma_N} \Delta n = V_{N\uparrow} - V_{N\downarrow} = \Delta V_N, \tag{4}$$

combining Ohm's law and Fick's law. The solution of the diffusion equations will be expressed in terms of the spin-splitting voltages to ensure straightforward comparison with experiments:

$$\Delta V_{Nx} = V_{Nx+} e^{-k_{N1}x} + V_{Nx-} e^{k_{N1}x}, \tag{5}$$

$$\Delta V_{Ny} = V_{Ny+} e^{-k_{N1}x} + V_{Ny-} e^{k_{N1}x}, \tag{6}$$

$$\Delta V_{Nz} = V_{Nz+} e^{-x/\lambda_N} + V_{Nz-} e^{x/\lambda_N}. \tag{7}$$

The spin-relaxation length is denoted by $\lambda_N = \sqrt{\tau_N D_N}$. The prefactors

$$V_{Nx+} = V_{N2+} \cos k_{N2}x + V_{N1+} \sin k_{N2}x, \tag{8}$$

$$V_{Nx-} = V_{N2-} \cos k_{N2}x - V_{N1-} \sin k_{N2}x, \tag{9}$$

$$V_{Ny+} = V_{N1+} \cos k_{N2}x - V_{N2+} \sin k_{N2}x, \tag{10}$$

$$V_{Ny-} = V_{N1-} \cos k_{N2}x + V_{N2-} \sin k_{N2}x, \tag{11}$$

contain the oscillating behavior of the spin-splitting voltages due to spin precession. The factors k_{N1} in the exponential functions and k_{N2} in the trigonometric functions are measures of the spin-relaxation and the spin-precession strength, respectively:

$$k_{N1} = \sqrt{\frac{1}{2D_N\tau_N}(1 + \sqrt{1 + \omega_L^2 \tau_N^2})}, \tag{12}$$

$$k_{N2} = \frac{\omega_L \tau_N}{\sqrt{2D_N\tau_N}} \frac{1}{\sqrt{1 + \sqrt{1 + \omega_L^2 \tau_N^2}}}. \tag{13}$$

The constants V_{N1+}, V_{N1-}, V_{N2+}, V_{N2-}, V_{Nz+}, and V_{Nz-} are evaluated employing the following boundary conditions: the spin-splitting voltages have to be zero in the bulk far away from the interfaces, and they have to be continuous at the interfaces. Furthermore the spin currents $\Delta I_N = I_{N\uparrow} - I_{N\downarrow}$ for each space direction have to be continuous. The spin currents are

$$\Delta I_{Nx} = +\frac{V_{Nx+}}{R_{N1}} e^{-k_{N1}x} - \frac{V_{Ny+}}{R_{N2}} e^{-k_{N1}x} - \frac{V_{Nx-}}{R_{N1}} e^{k_{N1}x} + \frac{V_{Ny-}}{R_{N2}} e^{k_{N1}x}, \tag{14}$$

$$\Delta I_{Ny} = +\frac{V_{Ny+}}{R_{N1}} e^{-k_{N1}x} + \frac{V_{Nx+}}{R_{N2}} e^{-k_{N1}x} - \frac{V_{Ny-}}{R_{N1}} e^{k_{N1}x} - \frac{V_{Nx-}}{R_{N2}} e^{k_{N1}x}, \tag{15}$$

$$\Delta I_{Nz} = \frac{\sigma_N S_N}{6\lambda_N} (V_{Nz+} e^{-x/\lambda_N} - V_{Nz-} e^{x/\lambda_N}). \tag{16}$$

The resistances R_{N1} and R_{N2} are defined as $R_{N1} = 6/(\sigma_N S_N k_{N1})$ and $R_{N2} = 6/(\sigma_N S_N k_{N2})$, where σ_N is the conductivity, and S_N is the cross-sectional area of the normal metal.

We assume single domain ferromagnets (F), i.e., only one direction exhibits a spin splitting due to exchange coupling. Therefore no spin precession occurs in the case of an undisturbed magnetization in low external magnetic fields. In experiments the alignment of the single domain is achieved by large shape anisotropy of the ferromagnetic electrodes. The diffusion equation, which describes the transport in the case of the ferromagnetic electrodes, reduces to

$$\frac{\Delta V_F}{\tau_F} = D_F \frac{\partial^2 \Delta V_F}{\partial x^2}. \tag{17}$$

ΔV_F is the spin-splitting voltage, τ_F is the spin-relaxation time, and D_F is the diffusion constant of the ferromagnetic metal. The general solution of Eq. (17) is

$$\Delta V_F = V_{F+} e^{-x/\lambda_F} + V_{F-} e^{x/\lambda_F}, \tag{18}$$

where $\lambda_F = \sqrt{\tau_F D_F}$ is the spin-relaxation length in the ferromagnet. The corresponding spin current is

$$\Delta I_F = \frac{1}{R_F} (V_{F+} e^{-x/\lambda_F} - V_{F-} e^{x/\lambda_F}), \tag{19}$$

where R_F is defined as $R_F = 2\lambda_F/[(1-\alpha^2)\sigma_F S_F]$, σ_F is the conductivity, and S_F is the cross-sectional area of the ferromagnet. In typical devices the spin-diffusion length in ferromagnetic materials (a few nm) is small in comparison to the side lengths of the contact areas (a few 100 nm). Thus there is spin-splitting in the ferromagnet only in the immediate

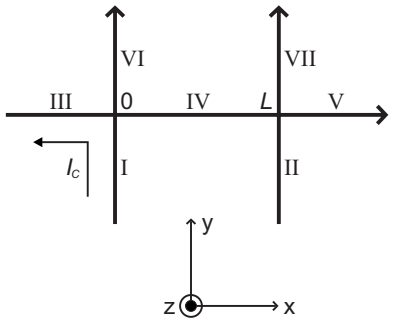

FIG. 1. Schematic spin-valve device subdivided into seven regions: regions I and VI denote the ferromagnetic injector electrode, regions II and VII are parts of the detector electrode, and regions III, IV, and V belong to the interconnecting normal metal strip. The electrode spacing is L. A current I_C is driven from region I to region III. The space directions are defined as shown in the coordinate system.

vicinity of the interface, and the size of the contact area should be used as S_F.

A tunnel barrier (I) at the interface between a normal and a ferromagnetic metal is also included in the present theoretical description by defining the spin-dependent contact conductivities per cross-sectional area

$$\Sigma_{C\uparrow} = \frac{(1+\beta)\Sigma_C}{2} \quad \text{and} \quad \Sigma_{C\downarrow} = \frac{(1-\beta)\Sigma_C}{2}. \tag{20}$$

Σ_C is the total conductivity per cross-sectional area of the tunnel barrier, and the parameter $\beta=(\Sigma_{C\uparrow}-\Sigma_{C\downarrow})/\Sigma_C$ describes the normalized difference in the conductivities for the spin-up and spin-down electrons. In general the spin polarization P of the current through the tunnel barrier is not equal to the parameter β and has to be evaluated for the distinct device geometry as will be discussed in Sec. II B. The tunnel barriers are assumed to be spin conserving and infinitely thin. The relation between the spin-splitting voltages ΔV_F and ΔV_N, and the spin current ΔI_{FIN} flowing through the interface from the ferromagnet to the normal metal is

$$\Delta V_F - \Delta V_N = R_C \Delta I_{\mathrm{FIN}}, \tag{21}$$

where R_C is defined by $R_C=2/[(1-\beta^2)S_C\Sigma_C]$ when S_C is the contact area of the interface.

In the following we discuss a spin-valve device consisting of two ferromagnetic electrodes and an interconnecting normal metal strip, which is subdivided into seven regions as shown in Fig. 1. The regions named I and VI denote the injector electrode, the regions II and VII are the detector electrode, and the normal metal strip consists of the regions III, IV, and V. The general solutions [Eqs. (5)–(7) and Eq. (18)] of the diffusion equations [Eqs. (1)–(3) and Eq. (17)] are adapted for each region separately regarding the above mentioned boundary conditions. A charge current I_C is driven from region I to region III. Concomitant spin-splitting voltages are obtained at the crossing between the left electrode and the normal metal strip. The magnetizations of the ferromagnetic electrodes are assumed to point in the y direction, resulting in a finite spin splitting Δn_y. The spin current and the spin-splitting voltages diffuse from the left crossing in all four directions especially toward the right crossing. At the right crossing a voltage difference due to the spin splitting can be measured between the normal metal strip and the right electrode in dependence on the magnetization of the right electrode. This is the so-called nonlocal measurement geometry.[1,4] During their journey through the normal metal a precession of the electron spins occurs due to the external magnetic field, which points in the z direction. For this geometry we have evaluated the spin-splitting voltages ΔV_{Nx} and ΔV_{Ny} in the normal metal in dependence on the strength of the external magnetic field.

A. Influence of spin precession

Application of the external magnetic field in the z direction induces spin precession in the normal metal strip. For the calculation of the spin-splitting voltages a typical set of parameters is used in accordance with our experiments: The conductivity of the aluminum $\sigma_N=2.0\times10^7\ \Omega^{-1}\ \mathrm{m}^{-1}$, the conductivity of the permalloy $\sigma_F=3.1\times10^6\ \Omega^{-1}\ \mathrm{m}^{-1}$, the average electrode spacing $L=820$ nm, the spin-relaxation time in aluminum $\tau_N=1.11\times10^{-10}$ s, the diffusion constant in aluminum $D_N=9.67\times10^{-3}\ \mathrm{m}^2\ \mathrm{s}^{-1}$, the normalized difference in the conductivities for the spin-up and spin-down electrons $\beta=0.35$, the spin-relaxation length in aluminum $\lambda_N=1034$ nm, and the current $I_C=50\ \mu$A. We take the bulk spin polarization $\alpha=0.35$ (Ref. 25), as well as the spin-relaxation length $\lambda_F=4.3$ nm (Ref. 26), which cannot be deduced from our experiments. We consider tunnel barriers at the interfaces with a total conductivity per cross-sectional area at the injector interface of $\Sigma_{C1}=4.6\times10^{10}\ \Omega^{-1}\ \mathrm{m}^{-2}$ and at the detector interface of $\Sigma_{C2}=3.7\times10^{10}\ \Omega^{-1}\ \mathrm{m}^{-2}$. The spin-splitting voltages are plotted along the lateral dimension of the normal metal in Fig. 2 for external magnetic fields of 0 mT (a), 50 mT (b), and 500 mT (c). The left electrode, where the current is injected, is located at $x=0$ and the detector electrode on the right at $x=820$ nm (see Fig. 1). Dashed and dotted lines in Fig. 2 are the voltages $V_{N\uparrow}$ and $V_{N\downarrow}$ of the spin-up and the spin-down electrons and the black and gray lines correspond to the spin-splitting voltages ΔV_{Ny} and ΔV_{Nx}. Figure 2(a) shows the well-known exponential decrease in the spin-splitting voltages in the absence of an external magnetic field and therefore without spin-precession. As the injected spins are parallel to the y axis, ΔV_{Nx} has to be zero. In an external magnetic field of 50 mT, see Fig. 2(b), the spin splitting in y direction is slightly reduced, and additionally a spin splitting in x direction occurs. The nonvanishing spin splitting in x direction ΔV_{Nx} at $x=0$ might be surprising if one has a ballistic picture in mind, but note that a diffusive approach in the steady state is used. In Fig. 2(c) the spin-splitting voltages at a relatively high external magnetic field of 500 mT are plotted. One observes the inversion of the spin-splitting voltages due to spin precession and a more pronounced exponential drop of the spin-splitting voltages due to the contribution of the Larmor frequency ω_L to the exponential factor k_{N1} (see Eq. (12)).

In the following the spin-splitting voltages

$$\Delta V_{Nx}(L) = \frac{Qe^{Lk_{N1}}(2\beta R_{C1} + \alpha R_{F1})\left[(2R_{C2} + R_{F2})\frac{R_{N1}}{R_{N2}}\cos(Lk_{N2}) + (2R_{C2} + R_{F2} + R_{N1})\sin(Lk_{N2})\right] I_C}{2e^{2Lk_{N1}}[Q(2R_{C1} + R_{F1}) + 1][Q(2R_{C2} + R_{F2}) + 1] - 2\left[\frac{R_{N1}}{R_{N2}}\sin(Lk_{N2}) - \cos(Lk_{N2})\right]^2} \tag{22}$$

and

$$\Delta V_{Ny}(L) = -\frac{Qe^{Lk_{N1}}(2\beta R_{C1} + \alpha R_{F1})(2R_{C2} + R_{F2})\left[\frac{R_{N1}}{R_{N2}}\sin(Lk_{N2}) - \cos(Lk_{N2})\right] I_C}{2e^{2Lk_{N1}}[Q(2R_{C1} + R_{F1}) + 1][Q(2R_{C2} + R_{F2}) + 1] - 2\left[\frac{R_{N1}}{R_{N2}}\sin(Lk_{N2}) - \cos(Lk_{N2})\right]^2} \tag{23}$$

in the normal metal at the detector electrode ($x=L$) are discussed with the abbreviation $Q=1/R_{N1}\cdot(1+R_{N1}^2/R_{N2}^2)$. The spin-splitting voltages at the detector electrode in dependence on the external magnetic field are shown in Fig. 3. Without an external magnetic field ΔV_{Nx} is zero, and ΔV_{Ny} is at its maximum. With increasing magnetic field an oscillatory behavior of the spin-splitting voltages is observed due to spin precession. The voltages show an exponential decrease toward higher magnetic fields because of the contribution of the Larmor frequency ω_L to the exponential factor k_{N1}. Consequently the spin-splitting voltages are attenuated at higher magnetic fields.

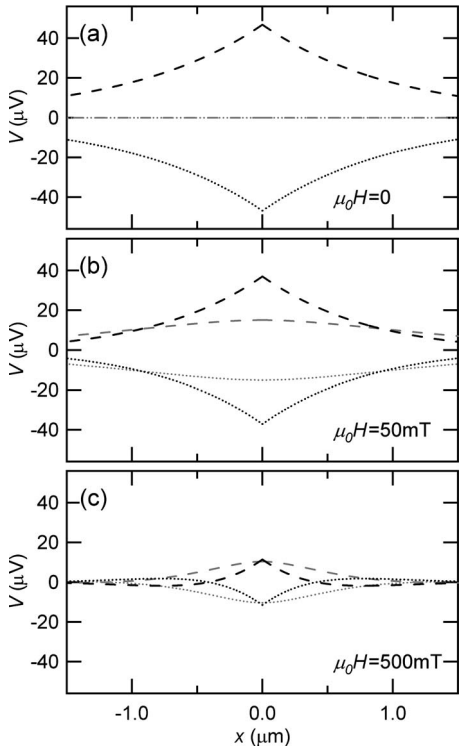

FIG. 2. Spin-splitting voltages along the normal metal. Three different external magnetic fields in the z direction have been assumed: (a) 0 mT, (b) 50 mT, and (c) 500 mT. Dashed and dotted lines are the voltages $V_{N\uparrow}$ and $V_{N\downarrow}$ of the spin-up and the spin-down electrons. Black and gray lines correspond to the spin-splitting voltages ΔV_{Ny} and ΔV_{Nx}, respectively. The parameters are $\alpha=0.35$ (Ref. 25), $\lambda_F=4.3$ nm (Ref. 26), $\sigma_N=2.0\times10^7\ \Omega^{-1}\ \mathrm{m}^{-1}$, $\sigma_F=3.1\times10^6\ \Omega^{-1}\ \mathrm{m}^{-1}$, $\Sigma_{C1}=4.6\times10^{10}\ \Omega^{-1}\ \mathrm{m}^{-2}$, $L=820$ nm, $\tau_N=1.11\times10^{-10}$ s, $D_N=9.67\times10^{-3}\ \mathrm{m}^2\ \mathrm{s}^{-1}$, $\beta=0.35$, $\lambda_N=1034$ nm, and $I_C=50\ \mu$A.

B. Influence of tunnel barriers

All calculations so far have been performed with tunnel barriers, which have a conductivity per cross-sectional area of about $4\times10^{10}\ \Omega^{-1}\ \mathrm{m}^{-2}$. The values have been obtained from measurements of the contact resistances. Tunnel barriers are known to enhance the spin-splitting voltages.[22] If the tunnel barriers are omitted a drastic decrease in the spin-dependent effects is expected. Figure 4 shows the spin-splitting voltages along the lateral dimension of the normal metal in the absence of tunnel barriers at the interfaces to the ferromagnetic electrodes. An external magnetic field of 50 mT is assumed. As expected the spin-splitting voltages are reduced by two to three orders of magnitude compared to the situation with tunnel barriers. The presence of tunnel barriers is crucial for the magnitude of the spin-splitting voltages for two reasons. First, a tunnel barrier between the injector electrode and the normal-metal strip potentially increases the spin-injection rate.[22] Note that the value of ΔV_{Ny} in Fig. 4 at $x=0$ is a factor of 400 smaller than in Fig. 2(b). Second, the tunnel barrier at the detector electrode strongly decreases the spin current into the electrode, which otherwise acts as a spin sink.[3,27,28] The spin-splitting is destroyed very fast in ferro-

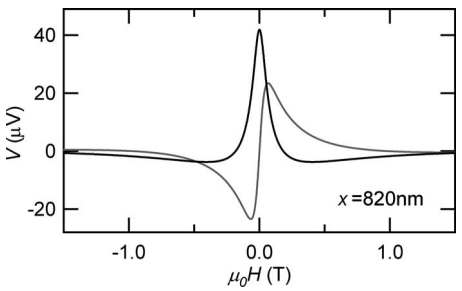

FIG. 3. Spin-splitting voltages ΔV_{Nx} (gray line) and ΔV_{Ny} (black line) at the detector electrode in dependence on the external magnetic field applied in the z direction. The set of parameters is specified in Fig. 2.

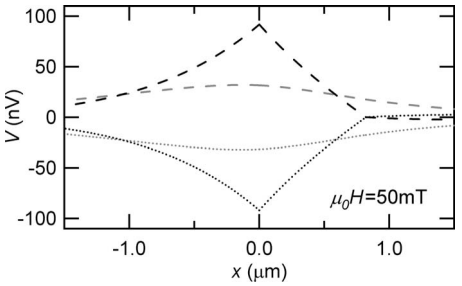

FIG. 4. Spin-splitting voltages in the normal metal without tunnel barriers at the interfaces to the ferromagnetic electrodes. The external magnetic field in the z direction is 50 mT. Dashed and dotted lines are the voltages $V_{N\uparrow}$ and $V_{N\downarrow}$ of the spin-up and the spin-down electrons. Black and gray lines correspond to the spin-splitting voltages ΔV_{Ny} and ΔV_{Nx}, respectively. The parameters are the same as in Figs. 2 and 3.

magnetic materials because of their small spin-relaxation lengths. Without tunnel barriers the spin current into the detector electrode intensifies the decrease in the spin-splitting voltage ΔV_{Ny} in the region of the normal metal between the injector and the detector electrode. This spin-sink effect can be seen in the pronounced asymmetry of ΔV_{Ny} around $x=0$ in Fig. 4. The spin-splitting voltage ΔV_{Nx} is not affected in the same manner because only electrons with a spin orientation in the y direction can diffuse into the detector electrode. A slight asymmetry is also observed in the shape of ΔV_{Nx} as both spin-splitting voltages are coupled via spin precession.

In the absence of a magnetic field the spin polarization of the current through the tunnel barrier into the normal metal reads for the present device geometry

$$P = \frac{2e^{2Lk_{N1}} \cdot [(\alpha R_{F1} + 2\beta R_{C1})(2R_{C2} + R_{F2} + R_{N1})]}{2e^{2Lk_{N1}} \cdot (2R_{C1} + R_{F1} + R_{N1})(2R_{C2} + R_{F2} + R_{N1}) - 2R_{N1}^2}. \tag{24}$$

The magnitude of the spin polarization P depends on tunnel barriers in the same way as the spin-splitting voltage ΔV_y. In the case of no tunnel barriers at the interfaces, the spin polarization P of the current injected into the normal metal has a value of $P=0.08\%$. Consideration of tunnel barriers at the F/N interfaces yields a spin polarization P of the current injected into the normal metal up to 34.4%.

III. SAMPLE PREPARATION

Spin-valve devices are fabricated in three steps using electron-beam lithography and lift-off processing. First the two permalloy electrodes are thermally evaporated on a high-resistance silicon substrate with a 300-nm thick silicon dioxide coating. The shorter and the longer electrode have lateral dimensions of 8 μm$\times$810 nm and 16 μm $\times$270 nm, respectively. Both electrodes have a thickness of 30 nm and consist of quasi single domains. This has been checked with magnetic-force microscopy in external magnetic fields at room temperature.[15,18] The spacing between the electrodes is 280 nm. Subsequently the aluminum strip is deposited on top of the electrodes using DC-magnetron sputtering. Between these two steps a tunnel barrier is formed either via natural oxidation in ambient air (sample SV9or) or in pure oxygen (sample SV33ur). For the latter process a cleaning of the surface by RF argon plasma etching is followed by deposition of aluminum. This aluminum finally is oxidized in pure oxygen at a pressure of 1 mbar for 15 min. From measurements of the current-voltage characteristic and the differential conductivity as a function of the bias voltage, the presence of tunnel barriers between the permalloy electrodes and the aluminum strip is confirmed. The data exhibits the characteristic shape for tunnel barriers as described by the theory of Brinkman.[29] The aluminum strip has a width of 550 nm and a thickness of 50 nm. Finally the permalloy electrodes are contacted with gold leads deposited by DC-magnetron sputtering. A scanning-electron micrograph of the device is shown in Fig. 5.

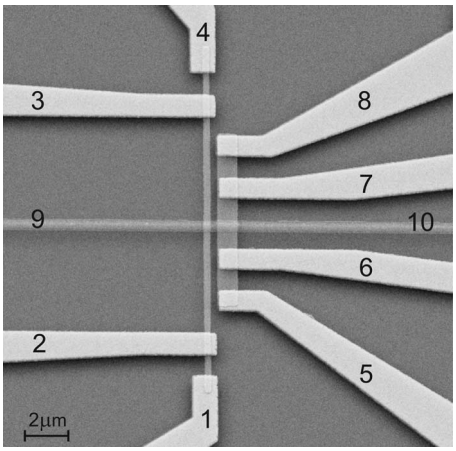

FIG. 5. Scanning-electron micrograph of a spin-valve device. Two permalloy electrodes are contacted via eight gold leads, numbered 1–4 and 5–8. The aluminum strip running from the left to the right is contacted via the leads 9 and 10.

IV. MAGNETOTRANSPORT MEASUREMENTS

All measurements have been performed at temperatures of liquid helium. The coercive fields of the two electrodes are determined via the anisotropic magnetoresistance.[18] In hysteresis loops slightly different values are found for each of the four coercive fields. The average values are -18 and 3 mT for the shorter and -25.0 and 13 mT for the longer electrode. All coercive fields observed are within a range of ± 2 mT around the average values. The significantly different switching fields of the electrodes are achieved by the large shape anisotropy of 4515 J m^{-3} and 8170 J m^{-3} of the shorter and the longer electrode, estimated in the Stoner–Wohlfarth[30] model with the standard saturation magnetization of 860 kA m^{-1} for permalloy. The coercive fields of both electrodes are not symmetric to zero field for two reasons: The superconducting solenoid, which produces the external magnetic fields has a remanence of 8 mT. Second, during and after the preparation process, the permalloy electrodes are oxidized at the surface at ambient air. This presumably produces a thin antiferromagnetic layer, which shifts the hysteresis loops by a few mT due to exchange-bias

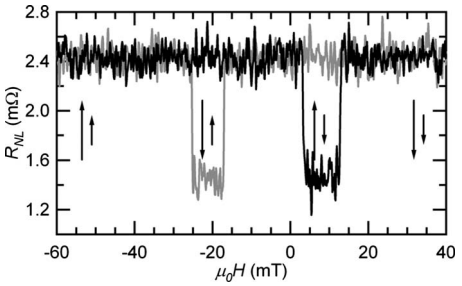

FIG. 6. Magnetoresistance of a spin valve recorded in the nonlocal measurement geometry (sample SV33ur), $I_C=50\ \mu$A. Black and gray lines denote the positive and negative sweep direction of the external magnetic field. Arrows indicate the magnetizations of the ferromagnetic electrodes.

coupling.[31] Furthermore an antiferromagnetic layer can cause spin scattering at the interface, which will influence the spin polarization of the current injected into the aluminum strip and will play a role in the nonlocal spin-valve measurements.

Spin-valve and spin-precession experiments have been performed in the nonlocal geometry, i.e., a current is sent from contact 2 to contact 9, and the voltage is probed at contacts 6 and 10 (see Fig. 5). This voltage between the aluminum strip and the detector electrode normalized with the charge current I_C is named the nonlocal resistance R_y and is connected to the spin-splitting voltage in the aluminum strip (Eq. (23)) via the relation

$$R_y(H) = \pm \frac{1}{2} \frac{2\beta R_C + \alpha R_F}{2R_C + R_F} \frac{\Delta V_{Ny}(L,H)}{I_C}. \tag{25}$$

The sign of R_y corresponds to the parallel or the antiparallel orientation of the magnetizations of the electrodes. In the measurements the nonlocal resistance is not symmetric around zero. For clarity we distinguish between the theoretical nonlocal resistance R_y and the observed nonlocal resistance with an offset R_{NL}. The spin-valve experiments have been performed with the external magnetic field applied parallel to the long axes of the electrodes, i.e., in y direction. In this case no spin precession occurs because the spins already point in the y direction, due to the magnetizations of the electrodes. The spin-valve effect is explained with the theoretical description by setting the external magnetic field to zero ($H=0$). Only two values are possible for R_y in accordance with the parallel and the antiparallel configuration of the magnetizations of the electrodes. The external magnetic field switches the magnetizations between these two states. The nonlocal magnetoresistance of a spin valve measured with a current amplitude of $I_C=50\ \mu$A at a temperature of 1.6 K is shown in Fig. 6. Black and gray lines denote the positive and the negative sweep direction of the external magnetic field. The phase of the signal of the LockIn amplifier is close to zero as it is expected for the low-modulation frequency of the present experiments (19 Hz). Following the magnetoresistance in the positive sweep direction of the external magnetic field, the signal remains on the same level as at negative saturation fields until the coercive field of the shorter electrode at 3 ± 2 mT is reached. Then the resistance drops to a lower level and remains the same up to the coercive field of the longer electrode at 13 ± 2 mT. Finally the resistance increases back to the initial level. The regions with increased resistance correspond to the parallel configurations of the magnetizations of the electrodes, and the regions with decreased resistance correspond to the antiparallel configurations. Note, that in the nonlocal measurement one obtains a pure spin-valve signal due to magnetization changes of the electrodes without contributions of parasitic effects such as the anisotropic magnetoresistance or the local Hall effect.[18] Minor loops have been recorded to support our interpretation and are displayed in Figs. 7(a) and 7(b), starting at negative and positive saturation fields, respectively. Following, e.g., the curves in Fig. 7(a) with a starting field at negative saturation, the resistance remains at the same level up to the positive coercive field of the shorter electrode and then drops to the resistance level of the antiparallel configuration of the magnetizations. The turning point of the sweep of the external magnetic field is between the coercive fields of both electrodes. While the external magnetic field is swept in the negative direction, the resistance remains at the decreased level until the negative coercive field of the shorter electrode is reached. Then the resistance increases back to its initial value at negative saturation fields. Thus only two parallel and two antiparallel alignments of the magnetizations are observed, resembling the genuine spin-valve behavior.

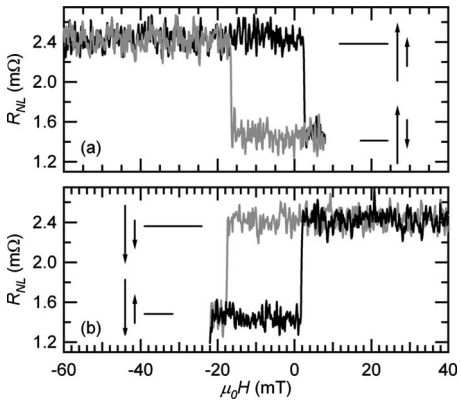

FIG. 7. Minor loops of the magnetoresistance starting at (a) negative and (b) positive saturation fields (sample SV33ur). Black and gray lines denote the positive and negative sweep direction of the external magnetic field. Arrows indicate the magnetizations of the ferromagnetic electrodes. The current amplitude was $I_C=50\ \mu$A.

Next the experiments on spin precession are presented. The external magnetic field is applied perpendicular to the sample plane in the z direction (see Fig. 1). Measurements are shown in Fig. 8(a). Black and gray lines correspond to the parallel and the antiparallel configuration of the magnetizations of the electrodes at zero field, respectively. In Fig. 8(b) offsets in the magnetic field and in the resistance have been subtracted for direct comparison to the theory.[32] In this graph the solid lines are fits to the measured data based on the theoretical description in Sec. II. Both sets of measured resistances exhibit an increase at magnetic fields larger than 100 mT, which is not included in the theory. This increase is

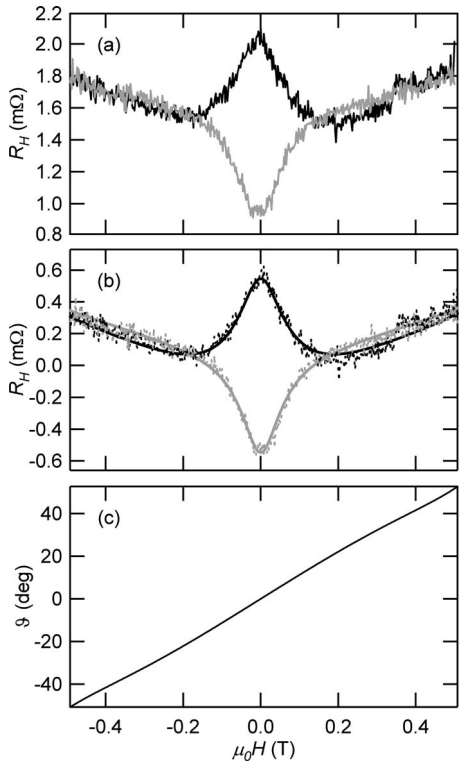

FIG. 8. (a) Magnetoresistance recorded in the nonlocal geometry with the external magnetic field pointing out-of-plane (z direction). Black and gray lines correspond to the parallel and the antiparallel orientation of the magnetizations of the electrodes at zero field, respectively (sample SV9or). (b) Offsets in the magnetic field of −8 mT and in the resistance of 1.478 mΩ have been subtracted from the experimental data.[32] The solid lines are fits according to Eq. (26). (c) Deduced angle ϑ between the easy axes of the electrodes and their magnetizations.

caused by the magnetizations of the electrodes that are reversibly turned away from the easy axes toward an out-of-plane state with increasing magnitude of the external magnetic field. In the limit of high magnetic fields (larger than 1.5 T), this results in an out-of-plane orientation of the magnetizations along the magnetic field in both electrodes. Therefore no spin precession occurs anymore. Thus the resistance saturates at the level of the parallel configuration of the magnetizations. This behavior can be described with the following relation:

$$R_H = R_y(H)\cos^2(\vartheta) + |R_y(H=0)|\sin^2(\vartheta), \qquad (26)$$

where ϑ is the angle between the easy axes of the electrodes and the magnetizations. This angle ϑ is zero at zero field and increases up to 90 degrees with increasing magnitude of the external magnetic field. The term $|R_y(H=0)|\sin^2(\vartheta)$ and therewith ϑ can be obtained by a polynomial fit to the arithmetic average of both experimental curves as $R_y(H)$ changes its sign when the magnetization configuration is switched from parallel to antiparallel. Thus the term $R_y(H)\cos^2(\vartheta)$ is eliminated in the arithmetic average. The polynomial fit has to be mirror symmetric to $H=0$ and was applied up to the sixth order. The angle ϑ in dependence on the external magnetic field is shown in Fig. 8(c). Its nearly linear increase confirms the description of the ferromagnets as single-domain electrodes. The results of the polynomial fit for $\vartheta(H)$ are used in the fit procedure of the measured resistances with Eq. (26). The following material parameters have been used for the fits: $\alpha=0.35$ and $\lambda_F=4.3$ nm have been taken from the literature.[25,26] The conductivities $\sigma_N=2.0\times10^7\ \Omega^{-1}\ \mathrm{m}^{-1}$, $\sigma_F=3.1\times10^6\ \Omega^{-1}\ \mathrm{m}^{-1}$, $\Sigma_{C1}=4.6\times10^{10}\Omega^{-1}\ \mathrm{m}^{-2}$, and $\Sigma_{C2}=3.7\times10^{10}\ \Omega^{-1}\ \mathrm{m}^{-2}$ have been determined from the sample. All cross-sectional areas have been deduced from the device geometry, and an average electrode spacing of 820 nm from the middle of one electrode to the middle of the other has been taken for L. τ_N, D_N, and β have been used as fit parameters resulting in $\tau_N=1.11\times10^{-10}$ s, $D_N=9.67\times10^{-3}\ \mathrm{m}^2\ \mathrm{s}^{-1}$, and $\beta=0.022$. This leads to a spin-relaxation length of $\lambda_N=1034$ nm.

V. DISCUSSION

The measured resistances of the spin valves in an out-of-plane applied external magnetic field are in very good agreement with our model presented in Sec. II. This proves the picture of precessing conduction electrons during their journey through the aluminum strip. In this model a spin-relaxation length of 1034 nm is deduced, which is in good agreement with other experiments.[6,7] Jedema *et al.*[6] have found spin-relaxation lengths between 600 and 1200 nm, depending on the conductivity of the aluminum in their samples: $\sigma_{Al}=1.7\times10^7\ \Omega^{-1}\ \mathrm{m}^{-1}$ and $\sigma_{Al}=8.0\times10^7\ \Omega^{-1}\ \mathrm{m}^{-1}$ at a temperature of 4.2 K, respectively. An increased conductivity yields a longer spin-relaxation length.

Although the nonlocal resistance should be symmetric in a fully nonlocal measurement, we observe an offset in the nonlocal resistance (see Fig. 6). In general, offsets, i.e., asymmetries in the spin-valve signals, can be explained by spin-dependent and spin-independent contributions. Spin-independent contributions can occur due to the sample geometry or the measurement setup.[33] A spin-dependent contribution emerges, e.g., from a third ferromagnetic or antiferromagnetic region that has a different magnetization behavior and has direct electrical contact to the voltage probes or the current. We have performed a fully nonlocal measurement and have observed a negligible phase, i.e., there should be no capacitive or inductive crosstalk. In a fully nonlocal measurement a homogeneous current distribution and a good quality of the interface are necessary for a symmetric nonlocal resistance and a high spin-valve efficiency. An antiferromagnetic layer, which is in electrical contact with the electrodes and with the interface to the tunnel barrier, might increase the interface resistance. This might produce an asymmetry in the nonlocal resistance. The observed shift of the switching fields mentioned in Sec. IV can also be caused by antiferromagnetic layers. In our device such layers could be in between the ferromagnetic electrodes and the tunnel barriers. The antiferromagnetic layers could have been formed by oxidation of the ferromagnetic electrodes in ambient air during the preparation process of sample SV9or. In the case of sample SV33ur the antiferromagnetic layers could have been formed by overoxidation of

the aluminum in pure oxygen.[34] An offset in the nonlocal resistance is a general feature observed in many measurements.[4,6,9,11–13,16,20,35] There have been speculations about its spin-dependent origin.[13] However, our results hint at a spin-independent contribution as source of the asymmetry. The antiferromagnetic layers break the symmetry of the nominally symmetric device. The symmetry breaking is mandatory to understand the offset in a nonlocal spin-valve signal.

We used the difference in the conductivities β for the spin-up and spin-down electrons as a third fit parameter besides the spin-relaxation time τ_N and the diffusion constant D_N of the normal metal, resulting in a value of $\beta=0.022$. By using Eq. (24) the spin polarization of the current through the tunnel barrier can be calculated and has a value of $P=2.16\%$. The value is in good agreement with Refs. 3, 4, and 11 and compared to Refs. 6, 8, and 12–14, a factor of two to three smaller. Exceptionally high values of 22.3% (at 79 K) and 25% (at 4.2 K) have been observed recently by Godfrey and Johnson,[35] and Valenzuela and Tinkham,[20] respectively, by integration of optimized tunnel barriers and interfaces. We suppose that the smaller spin polarization of the current injected in the normal metal reflects pronounced spin-scattering at the interfaces in our device. The scattering is presumably caused by the above-mentioned antiferromagnetic layer on top of the permalloy electrodes.

VI. CONCLUSION

We have experimentally studied spin diffusion, spin precession, and spin relaxation in all-metal spin valves using their unique sensitivity to the spin degree of freedom. The diffusion equations including spin precession, tunnel barriers at the interfaces, and spin-relaxation processes were solved for the present spin-valve device geometry using the conductivities determined from our transport experiments. In particular, for a spin valve with tunnel barriers at the interfaces between the ferromagnetic electrodes and the normal metal strip, formulas for the spin-splitting voltages in the normal metal at the detector electrode and the resulting nonlocal magnetoresistance were deduced. The spin-splitting voltages in the whole aluminum strip that result from spin precession in external magnetic fields have been analyzed. The influence of tunnel barriers at the interfaces between the ferromagnets and the normal metal strip has been discussed. We have shown that tunnel barriers are essential to improve the spin injection and to avoid the spin-sink effect at the detector electrode. Measurements of the spin-valve effect and of spin precession at temperatures of liquid helium are well described by the model. The spin-diffusion length in aluminum ($\lambda_{Al}=1034$ nm) and the spin polarization injected into the normal metal strip ($P=2.16\%$) obtained by fitting our measurements with the model are in concordance with previously published data. We observed an asymmetry in the nonlocal resistance that is found with varying values in other publications as well. Our results indicate a symmetry breaking caused by an antiferromagnetic layer that is in electrical contact with the electrodes.

ACKNOWLEDGMENTS

We would like to thank B. J. van Wees and T. Matsuyama for fruitful discussions, as well as J. Gancarz for superb technical assistance. Financial support from the Sonderforschungsbereich 508 "Quantenmaterialien" is gratefully acknowledged.

*jwulfhor@physnet.uni-hamburg.de

[1] M. Johnson and R. H. Silsbee, Phys. Rev. Lett. **55**, 1790 (1985).
[2] M. Johnson and R. H. Silsbee, Phys. Rev. B **37**, 5326 (1988).
[3] M. Johnson and R. H. Silsbee, Phys. Rev. B **37**, 5312 (1988).
[4] F. J. Jedema, A. T. Filip, and B. J. van Wees, Nature (London) **410**, 345 (2001).
[5] F. J. Jedema, M. S. Nijboer, A. T. Filip, and B. J. van Wees, J. Supercond. **15**, 27 (2002).
[6] F. J. Jedema, H. B. Heersche, A. T. Filip, J. J. A. Baselmans, and B. J. van Wees, Nature (London) **416**, 713 (2002).
[7] F. J. Jedema, M. S. Nijboer, A. T. Filip, and B. J. van Wees, Phys. Rev. B **67**, 085319 (2003).
[8] M. Zaffalon and B. J. van Wees, Phys. Rev. Lett. **91**, 186601 (2003).
[9] T. Kimura, J. Hamrle, and Y. Otani, Phys. Rev. B **72**, 014461 (2005).
[10] S. Hershfield and H. L. Zhao, Phys. Rev. B **56**, 3296 (1997).
[11] Y. Ji, A. Hoffmann, J. S. Jiang, and S. D. Bader, Appl. Phys. Lett. **85**, 6218 (2004).
[12] Y. Ji, A. Hoffmann, J. E. Pearson, and S. D. Bader, Appl. Phys. Lett. **88**, 052509 (2006).
[13] S. Garzon, I. Žutić, and R. A. Webb, Phys. Rev. Lett. **94**, 176601 (2005).
[14] M. Zaffalon and B. J. van Wees, Phys. Rev. B **71**, 125401 (2005).
[15] A. van Staa, C. M. S. Johnas, U. Merkt, and G. Meier, Superlattices Microstruct. **37**, 349 (2005).
[16] T. Kimura, Y. Otani, and J. Hamrle, Phys. Rev. Lett. **96**, 037201 (2006).
[17] J. Ku, J. Chang, S.-H. Han, J. G. Ha, and J. Eom, J. Magn. Magn. Mater. **304**, e273 (2006).
[18] A. van Staa and G. Meier, Physica E (Amsterdam) **31**, 142 (2006).
[19] T. Kimura and Y. Otani, J. Appl. Phys. **101**, 126102 (2007).
[20] S. O. Valenzuela and M. Tinkham, Appl. Phys. Lett. **85**, 5914 (2004).
[21] A. Fert and H. Jaffrès, Phys. Rev. B **64**, 184420 (2001).
[22] E. I. Rashba, Phys. Rev. B **62**, R16267 (2000).
[23] P. C. van Son, H. van Kempen, and P. Wyder, Phys. Rev. Lett. **58**, 2271 (1987).
[24] G. Schmidt, D. Ferrand, L. W. Molenkamp, A. T. Filip, and B. J. van Wees, Phys. Rev. B **62**, R4790 (2000).
[25] L. Bocklage, J. M. Scholtyssek, U. Merkt, and G. Meier, J. Appl. Phys. **101**, 09J512 (2007).
[26] S. Dubois, L. Piraux, J. M. George, K. Ounadjela, J. L. Duvail, and A. Fert, Phys. Rev. B **60**, 477 (1999).

[27] Y. Tserkovnyak, A. Brataas, and G. E. W. Bauer, Phys. Rev. Lett. **88**, 117601 (2002).
[28] M. D. Stiles and A. Zangwill, Phys. Rev. B **66**, 014407 (2002).
[29] W. F. Brinkman, R. C. Dynes, and J. M. Rowell, J. Appl. Phys. **41**, 1915 (1970).
[30] E. C. Stoner and E. P. Wohlfarth, Philos. Trans. R. Soc. London, Ser. A **240**, 599 (1948).
[31] T. Last, S. Hacia, S. F. Fischer, and U. Kunze, Physica B (Amsterdam) **384**, 9 (2006).
[32] The offset in the magnetic field of −8 mT is caused by the remanence of the superconducting solenoid. The offset in the resistance cannot be explained by the theory, which predicts a change in the sign between the parallel and the antiparallel orientation of the magnetizations of the electrodes. A resistance offset of 1.478 mΩ has to be subtracted so that the two curves are symmetric in the range between ±50 mT.
[33] N. Tombros, C. Jozsa, M. Popinciuc, H. T. Jonkman, and B. J. van Wees, Nature (London) **448**, 571 (2007); B. J. van Wees (private communication).
[34] H. Boeve, J. De Boeck, and G. Borghs, J. Appl. Phys. **89**, 482 (2001).
[35] R. Godfrey and M. Johnson, Phys. Rev. Lett. **96**, 136601 (2006).